ELSEVIER

Journal of Fluids and Structures 21 (2005) 133–149

JOURNAL OF FLUIDS AND STRUCTURES

www.elsevier.com/locate/jfs

Influence of the nature of the gas in the edge-tone phenomenon

J.F. Devillers[1], O. Coutier-Delgosha*,[2]

ENSTA, UER de Mécanique, Chemin de la Hunière, 91761 Palaiseau cedex, France

Received 27 July 2004; accepted 17 July 2005
Available online 3 October 2005

Abstract

The present study deals with the edge-tone phenomenon. Gas injection is performed through a nozzle with a $0.6 \times 20\,mm^2$ cross-section and two possible lengths of 20 and 50 mm. The effect of the nature of the injected gas on both the flow arrangement and sound frequency is investigated by a coupled experimental and numerical approach. In the experiments, special attention is paid to the definition and experimental measurement of the velocity at the nozzle outlet for the three injected gases. If the head losses in the injection duct are correctly taken into account, no influence of its length is obtained, which contradicts the results published recently by Ségoufin et al. [2004. Experimental investigation of the flue channel geometry influence on edge-tone oscillations. Acta Acustica 90, 966–975]. Injections of air, Neon, and CO_2 into air are then successively considered. The numerical simulations are based on the two-dimensional resolution of the unsteady Navier–Stokes equations, in association with a two-fluid physical model. A homogeneous approach is used to treat the behaviour of the mixture composed of the two gases. The density of the injected gas is found to have a significant influence on the flow pattern and the sound frequency, which suggests that the fluid density should be included in the relations that give the frequency of the edge tone instability. Moreover, it is shown that the jet oscillation frequencies obtained both numerically and experimentally can be derived from a theoretical analysis of the Kelvin–Helmholtz instability, on condition that the parabolic shape of the gas velocity at the nozzle outlet is taken into account.

1. Introduction

The edge-tone phenomenon consists in the interaction of a jet with an obstacle located downstream, resulting in a tone with discrete frequencies. A typical situation for the edge-tone phenomenon is shown in Fig. 1 in the case of a plane jet interacting with a wedge. The sound emission is due to the flow destabilization and the formation of vortices on both sides of the wedge. This phenomenon is based on the excitation of the unstable shear layers near the lips of the injection pipe. The disturbances are then convected downstream to the edge and amplified by a feedback loop into coherent and large-scale vortices, as first suggested by Powell (1953). Edge-tones are often used to initiate the vibratory phenomena in musical wind instruments (recorders, flue organ pipes). It is also involved in industrial mechanisms, such as modern gas

*Corresponding author.
E-mail addresses: devilJF@aol.com (J.F. Devillers), olivier.coutier@lille.ensam.fr (O. Coutier-Delgosha).
[1]Now Scientific Consultant, 4 rue Mirabeau, 91120 Palaiseau, France.
[2]Now at ENSAM Lille/LML laboratory, 8 bld Louis XIV, 59046 Lille cedex, France.

0889-9746/$ - see front matter © 2005 Elsevier Ltd. All rights reserved.
doi:10.1016/j.jfluidstructs.2005.07.003

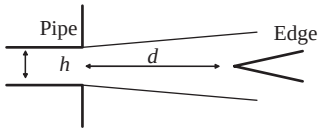

Fig. 1. Edge-tone phenomenon.

flow-meters with no mechanical part in motion; some of them are based on measurement of the vortex-shedding frequency associated with edge-tone phenomenon (Maurel et al., 1996).

A concordant analogy between the vortex street of the edge-tone and the Karman one has been proposed first by Benton (1925) on the basis of experimental measurements. More recently, the theoretical developments performed by Holger et al. (1977) and Howe (1998) have confirmed the analogy. Several scaling laws derived from experimental or theoretical work have also been proposed to fit the dependency of the oscillation frequency f on the parameter h/d (Holger et al., 1977; Crighton, 1992; Howe, 1998), where h is the nozzle height and d denotes the stand-off distance between the nozzle outlet and the wedge. These authors propose the following general form for the relation between the Strouhal number $\mathrm{St} = fh/V_{\mathrm{ref}}$ and h/d:

$$\mathrm{St} = C(h/d)^n, \tag{1}$$

where n equals 3/2, and the laws differ from one another through the constant C, only. It can be remarked that the density of the injected gas does not appear in these relations, so it can be expected that the gas density will have no influence on the Strouhal numbers when the ratio d/h is fixed. The same assumption is implicitly made concerning the flow arrangement and the shape of the vortices on the sides of the wedge: in the literature, indeed, quantitative measurements performed in air are often illustrated with flow visualizations obtained by the "Schlieren" method with injection of a gas with a different density, for example CO_2 (Maurel et al., 1996; Ségoufin et al., 2004).

However, no evidence for this has ever been established, although it may be a noteworthy parameter in the study of flute-like instruments. As a matter of fact, the air expired by a musician contains nearly 6% of water vapour and 3% of CO_2, while standard air contains only 1% of vapour and 0.03% of $C0_2$. The densities of these two gases are different from that of air, so the frequencies of the emitted sound in real conditions may be notably different from the results of theoretical or experimental studies performed with standard air injection. Significant pressure and temperature variations may also slightly modify the air density, and thus affect the sound of these wind instruments.

In the present paper, the influence of the nature of the injected gas on the vortex-shedding phenomenon is investigated. The edge-tone is obtained by injecting gas through a nozzle located at a distance d from the edge. The width b of the pipe is much larger than its height h; thus the flow can be considered as nearly two-dimensional (2-D). The velocity distribution at the nozzle outlet is a key point of the experimental set-up, since it may act on the vibratory properties of the flow. Two types of distributions are usually considered: the established velocity profiles with a nearly parabolic distribution in the core (Bickley shape), and the ones with a zone of constant velocity towards the axis (top hat). The two configurations essentially result from the shape factor of the pipe, i.e. the ratio h/L, where L is the pipe length. In the present study, L is large enough to systematically obtain a parabolic velocity distribution at the nozzle outlet (Schlichting, 1979). The flow remains laminar, since the Reynolds number $\mathrm{Re} = V_{\mathrm{ref}}D/\nu$ never exceeds 600, where V_{ref} denotes the mean velocity at the pipe outlet and D is the hydraulic diameter $D = 2bh/(b+h)$.

Injections into air of three gases, namely air, Neon, and carbon dioxide (CO_2), are successively performed to study the influence of the gas density. The determination of the reference velocity in these different cases requires the previous calculation of the losses in the pipe. As a matter of fact, it is common to see in the literature the reference velocity of the flow simply calculated with the Bernoulli formula, based on the difference between the upstream total pressure in the chamber and the static pressure, which is generally the atmospheric pressure (Ségoufin et al., 2000, 2004). However, head losses become preponderant when the length L of the pipe is increased, and they also depend significantly on the gas density: in the extreme case of pure Neon or CO_2 injection, it is obvious that the head loss in the duct will be different from the case of air injection. In the case of a mixture of several gases, the head loss is a function of the concentration. Therefore, the determination of the losses in the pipe is a necessary first step to investigate the effect of the gas nature on the frequency of the vortices.

Numerical simulations of the unsteady flow around the edge are also performed with a two-dimensional model based on finite volume discretization of the Navier–Stokes equations. A two-phase model is used in the simulations, in order to simulate injection of Neon or CO_2 into air. No turbulence model is applied, so only the characteristics of flow destabilization before the transition to turbulence are considered. The objective is to validate the model by comparing predicted to measured shedding frequencies.

Sections 2 and 3 of the paper present the experimental set-up and the measuring techniques, and the numerical model, respectively. Section 4 is devoted to the calibration of the experimental device with: (i) the verification of classical behaviour, such as the decrease of the shedding frequency when the edge/nozzle distance is increased, or its increase proportionally to the jet velocity; (ii) the calculation of the pressure losses in the pipe when air, CO_2 or Neon are injected; (iii) the validation of the measurements in air. Then, Section 5 presents the numerical and experimental results with air, Neon, and CO_2 injection at the two first frequency stages. Finally, in Section 6 a theoretical analysis of the edge-tone phenomenon is reported, based on the linear analysis of the Kelvin–Helmholtz instability. Indeed, injections of gases different from air lead, on both sides of the jet, to conditions that can be considered similar to such an instability. The objective is to recover by the theory the results obtained both numerically and experimentally, by taking the velocity and density distributions at the pipe outlet into account in the analytical development.

2. Experimental set-up

Experiments were conducted in a plexiglas model including a tranquilization (settling) chamber and a converging nozzle leading to an interchangeable rectangular flue with length $L = 50$ or 20 mm and height $h = 0.6$ mm. The chamber dimensions are large enough to ensure velocities almost equal to zero therein. The effective transverse size of the model is $b = 20$ mm. So $b/h = 33 \gg 1$, and the flow will be considered as two-dimensional. The wedge, whose dimensions are 20 mm × 6 mm (see Fig. 2(a)), faces the pipe outlet and is held in this position by two side plates, as shown in Fig. 2(b). It can be moved in the flow direction by precision grooves and a micrometric screw. The distance d between the nozzle outlet and the edge will be varied between 3 and 5 mm in the experiments. Two wide circular openings were cut in the side plates around the obstacle leading edge to avoid any acoustic confining and to enable good optical quality for flow visualizations.

Flow visualizations were performed by a standard Schlieren technique (Merzkirch, 1987; Yoshikawa, 2000) when CO_2 or Neon is injected. This method is based on the fact that the refractive index of a medium depends on its local density. Thus, if a flow with variable density is illuminated, brightness variations proportional to density gradients are obtained. In the present case, a classical optical bench is used in order to visualize CO_2 or Neon vortices around the edge. The model is located perpendicularly to the optical axis between two converging lenses whose focal length is about 1 m. The light source is a 1 mm diameter hole in an opaque plate lying in the collimated image plane of a stroboscopic lamp. At the other end, a standard CCD camera is focused on the flow. The camera is connected to a PC for data acquisition, and the image processing is performed with the software OPTIMAS. An example of flow visualization is given in Fig. 3 in the case of CO_2 injection. The compressed air source is the laboratory network, while CO_2 and Neon are stored in bottles. The three parallel feedings are connected to the duct going towards the settling chamber upstream from the injection flue. So, the gas nature can easily be changed and mixing of the gases can also be obtained. For each gas, the upstream pressure is controlled by a pressure reducer and an adjustable valve. It has been checked for the three gases that the temperature at the nozzle outlet remains constant, for all the flow velocities that are investigated in the present work.

The experimental bench is fitted out with various means of measurement. A 1/4″ free-field Electret microphone (sensitivity 4.94 mV/Pa), located approximately 2 cm under the edge, enables to perform the spectral analysis of the tone. The precision of the characteristic frequency mainly depends on the frequency discretization, which is here $\Delta f = 15$ Hz. The velocity field in air (mean values and fluctuations) can be obtained by hot-wire anemometry, using a Dantec 55P14 probe whose diameter is 5 μm and a Dantec 55M05 bridge. Such a probe can be used confidently for velocities higher than 1 m/s, which is the case here. This is a first way to obtain in air the value of the mean velocity V_{ref}.

Moreover, two pressure values are available: the first one P_1 inside the settling chamber before the pipe, and the second one P_2 at the pipe exit where a mini Pitot probe (0.2 mm interior diameter and 0.6 mm exterior one) is located. This probe enables us to measure the maximum total pressure P_2 in the jet and thus to estimate the maximum velocity V_{max} at the pipe outlet. Assuming that the velocity distribution is parabolic (this point will be checked in Section 4), then the mean velocity V_{ref} can be derived from the relation

$$V_{ref} = \frac{2}{3}\sqrt{2\frac{P_2}{\rho}}. \tag{2}$$

Two Keller model PD-11-0.1 differential pressure transducers with sensitivity 0.007 mV/Pa are used for pressure measurements. The precision mainly depends on the transducer calibration, and it is estimated here to 0.5 mm of water, i.e. ±5 Pa. A micrometric displacement system (precision 2 μm) is used for both hot-wire and Pitot probes.

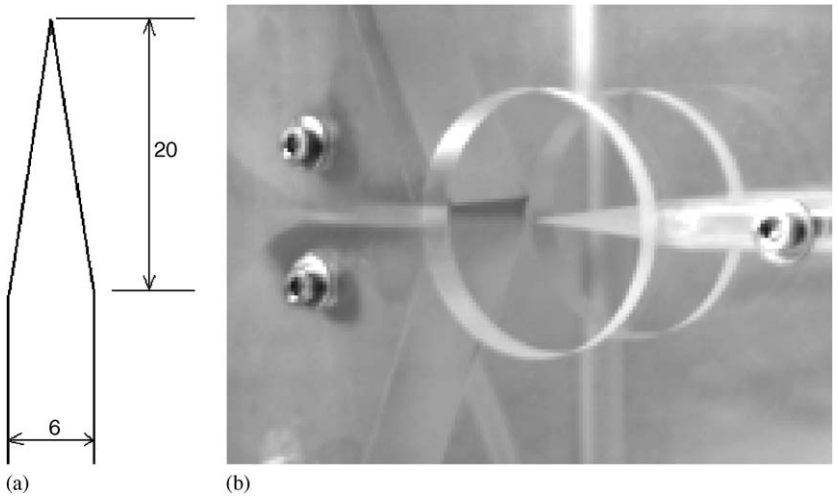

Fig. 2. Flow configuration: (a) dimensions of the edge in mm and (b) view of the test model.

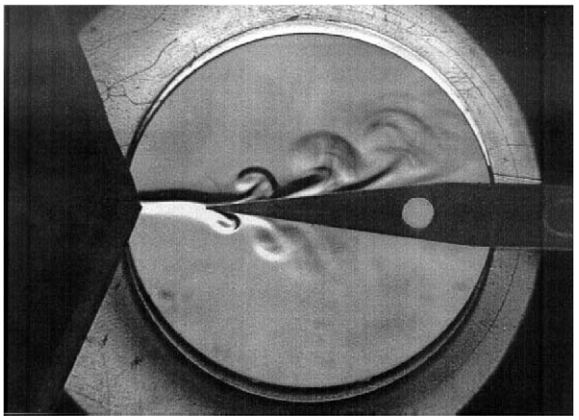

Fig. 3. Visualization of the flow vortices by the Schlieren technique (CO_2 injection).

3. Numerical model

The numerical simulations are based on the coupling between the resolution of the Navier–Stokes equations with a supplementary physical model that controls the concentration of the different gases in the flow field. The details of the model are given by Coutier-Delgosha et al. (2005), and only the main features are indicated below.

3.1. Two-fluid physical model

We consider hereafter the injection of a gas that is possibly different from air, denoted as "gas_1", into the air, denoted as "gas_2". The two gases are characterized, respectively, by densities ρ_1 and ρ_2 and by dynamic viscosities μ_1 and μ_2, which are all supposed to be constant. In the present approach the flow is supposed to be composed of a single fluid whose density varies from ρ_1 to ρ_2 and viscosity from μ_1 to μ_2 according to the local ratio $\alpha = V_1/V$, where V_1 denotes the volume occupied by the gas_1 in a cell whose total volume is V. So the gas_1/gas_2 mixture is considered as a homogenous medium whose properties depend on the local value of α. The evolution of α is controlled by a transport equation issued from the mass balance equation for gas_1,

$$\frac{\partial \alpha}{\partial t} + \nabla \cdot (\alpha \boldsymbol{u}) = 0, \tag{3}$$

where $\boldsymbol{u}$ denotes the medium velocity, considering no slip between the two gases. This is a reasonable assumption, since gas_1 and gas_2 are characterized by very close properties (perfect gases). Eq. (3) is coupled to the balance equations for the mixture, which can be expressed as

$$\frac{\partial \rho}{\partial t} + \nabla \cdot (\rho \boldsymbol{u}) = 0, \tag{4}$$

$$\frac{\partial (\rho \boldsymbol{u})}{\partial t} + (\boldsymbol{u} \cdot \nabla)\rho \boldsymbol{u} = \mu \Delta \boldsymbol{u}$$

with $\rho = \alpha\rho_1 + (1-\alpha)\rho_2$ and $\mu = \alpha\mu_1 + (1-\alpha)\mu_2$ if considering a linear variation for simplicity.

3.2. Numerical resolution

No thermal effects are considered in the present study (see Section 2), so the energy equation is not resolved. The flow is considered as two-dimensional and fully laminar, which is consistent with the experimental conditions reported in Section 2. The transition to turbulence that is observed sometimes experimentally along the edge is thus not modeled. However, this transition is obtained only for high injection flow rate and it never affects the first vortices on each side of the edge. Thus, we suppose that it has little influence on both the shedding frequency and feedback mechanism.

Eqs. (3) and (4) are written in the orthogonal frame of curvilinear coordinates (ξ,η), which leads to the following expression proposed initially by Pope (1978):

$$S\frac{\partial}{\partial t}(\rho \Phi) + \nabla_\xi \left(\rho u \Phi - \Gamma_\Phi \frac{\partial \Phi}{\partial \xi} \right) + \nabla_\eta \left(\rho v \Phi - \Gamma_\Phi \frac{\partial \Phi}{\partial \eta} \right) = S_\Phi, \tag{5}$$

where Φ stands for 1, u, v, *or* α; Γ_Φ is the diffusion coefficient; u and v are the velocity components along coordinates ξ and η, respectively; ∇_ξ and ∇_η are the physical components of the divergence operator along the curvilinear coordinates, and S_Φ is the source term.

The finite volume method is used for space discretization. Each equation is integrated locally on its own control volume based on the staggered grid to avoid pressure oscillations. The pressure, the density and α are calculated at the centre of the cells, while the velocity components u and v are located on the western and the southern faces of each cell, respectively. The divergence term in Eq. (5) is first transformed into a sum of fluxes through the control volume faces. The diffusive terms are then discretized in a purely central manner, while the convection terms are estimated through the HLPA scheme proposed by Zhu (1991). This results in a second-order scheme, which locally switches to first order, to prevent numerical oscillations in critical high-pressure gradient areas.

An unconditionally stable, second-order implicit scheme is applied for time discretization, leading to the following expression for the time-dependent terms:

$$\frac{\partial(\rho \Phi)}{\partial t} = \frac{1.5\rho^{n+1}\Phi^{n+1} - 2\rho^n \Phi^n + 0.5\rho^{n-1}\Phi^{n-1}}{\Delta t}. \tag{6}$$

The numerical resolution is based on the pressure-correction method proposed by Patankar (1981).

3.3. Calculations

All simulations are performed in the geometrical configuration $d = 4\,\text{mm}$. Classical boundary conditions are applied: imposed inlet velocity, and fixed outlet pressure. A constant pressure is also imposed along the two horizontal boundaries. A parabolic velocity distribution is imposed at the inlet to be consistent with the experimental flow conditions. The computational domain (Fig. 4) is composed of 500×200 cells, with a special grid contraction close to the edge walls (in the vertical direction) and between pipe and edge (horizontal direction). A supplementary contraction is also imposed vertically downstream from the pipe aperture to avoid numerical dissipation of the velocity profile before the obstacle leading edge. A grid stretching is imposed close to the boundary to guarantee the dissipation of the vortices before they reach the frontiers of the computational domain.

A time step is considered as converged when the nondimensional residuals of all equations, which are defined as the sum of the residuals in each cell of the domain, have fallen under 10^{-3}. A supplementary criterion is also included concerning the sum of the density variations, which must decrease below 10^{-5}. A maximum number of 500 iterations

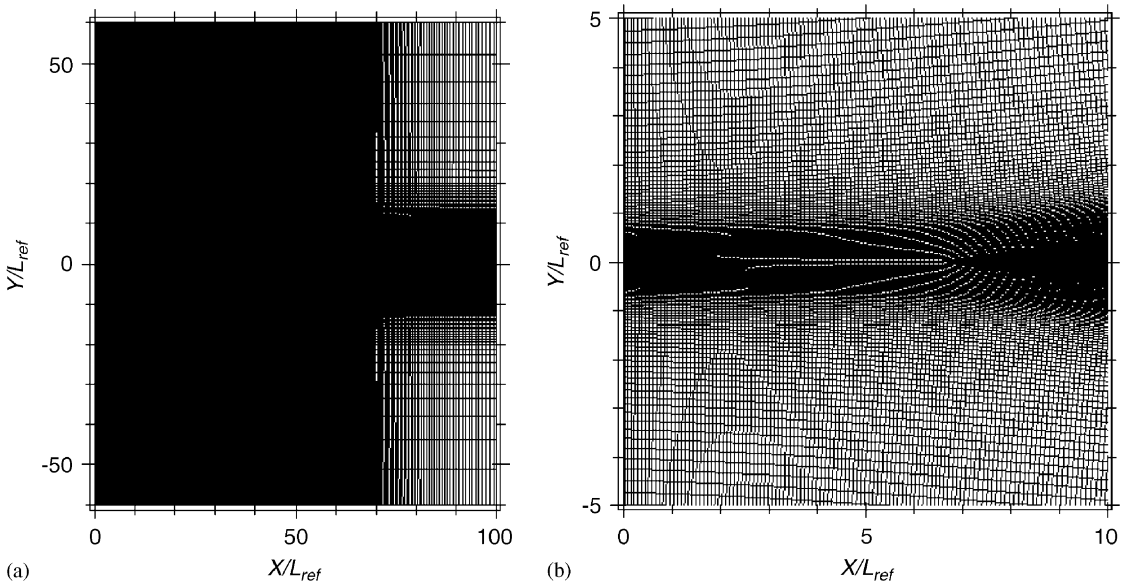

Fig. 4. Computational domain: (a) general view and (b) detail between the pipe and the edge.

Table 1
Effects of the grid size and the time step on the frequency f predicted by the simulations (no wedge, Neon injection, $V_{ref} = 5\,m/s$)

$\Delta t/T_{ref}$	Grid size	f (Hz)
0.02	500×200	170
0.05	500×200	165
0.1	500×200	170
0.2	500×200	172
0.1	200×80	205
0.1	400×150	180
0.1	1000×300	173

per time step are allowed. However, in all the present calculations, the time-steps were systematically converged, according to the previous criteria.

The standard value of the time-step applied for the calculations is $\Delta t = T_{ref}/10$, where $T_{ref} = L_{ref}/V_{ref}$ with $L_{ref} = 0.6\,mm$ (the pipe height) and V_{ref} the mean flow velocity at the nozzle outlet. The simulation is performed during $600T_{ref}$, which is sufficient here to characterize the unsteady flow and calculate the shedding frequency. No perturbation was applied to initiate the flow unsteadiness. Influence of the numerical parameters has been tested in a configuration of air injection with no wedge. In this situation, a transition from laminar to turbulent flow is observed in the experiments. Before the transition, a first instability characterized by periodic emission of vortices is observed. The capability of the numerical model to reproduce this instability has been checked, and the detailed results are reported by Coutier-Delgosha et al. (2005). In the present paper, only the results concerning the influence of the grid dimensions and the time step are given in Table 1. Four grid sizes have been tested: 200×80, 400×150, 500×200 and 1000×300. The nondimensional time step $\Delta t/T_{ref}$ has been varied between 0.02 and 0.2. Neon injection is performed in all cases, with a reference velocity $V_{ref} = 5\,m/s$. The frequency measured in the experiment for these flow conditions is 167 Hz, and the frequencies obtained in the simulations are reported in Table 1. It can be observed that the time step has nearly no influence on the result. The grid size has also a very small influence, except in the case of the coarsest mesh, that leads to a frequency significantly too high. The dimension 500×200 was finally found to be the best compromise for accuracy/computational-cost.

4. Experimental results

4.1. Verification of classical results

The experimental results reported in the present section were obtained without considering any head loss in the pipe. Thus the reference jet velocity is calculated with the Bernoulli perfect fluid formula, based on the difference between the upstream pressure in the settling chamber and the one at the nozzle outlet, which is the atmospheric pressure. This method is the one often reported in previous papers concerning edge-tone experiments (Ségoufin et al., 2000, 2004). In their most recent paper, these authors have tested several shapes and lengths for the injection duct, and they conclude that these parameters have much influence on the Strouhal numbers.

Several flow conditions are investigated in the present study by injecting air and varying the upstream pressure. Three values of d (distance of pipe to wedge) are considered, and the frequency f of the vortex shedding is plotted in Fig. 5 as a function of the flow reference velocity. The two first frequency stages are considered here. A linear variation of the frequency is obtained between two jumps in the three geometrical configurations. The classical hysteresis phenomenon between the frequency jumps (Brown, 1937) is also observed, and it is clearly amplified when the value of d is reduced.

Although these standard behaviours are correctly obtained, it can be noticed that all the curves converge towards a constant nonzero value of the velocity slightly lower than 10 m/s. This trend is in contradiction with the conclusions of Holger et al. (1977), Howe (1998) and Crighton (1992), who all report nearly constant Strouhal numbers (nondimensional frequency $\mathrm{St} = fh/V_{\mathrm{ref}}$ or $\mathrm{St} = fd/V_{\mathrm{ref}}$) when the ratio d/h is fixed. In other words, the shedding frequency is proportional to the reference jet velocity. The same property is observed in the so-called Karman wakes for a wide range of Reynolds numbers, above the critical value.

This discrepancy suggests that the head losses in the injection duct cannot be neglected in the present case. To confirm this point that basically depends on the pipe form factor, hot-wire velocity measurements were performed in air at the flue outlet. The wedge was removed to enable the use of the hot-wire probe a few millimetres after the pipe aperture. The result is presented in Fig. 6 in the case of a reference velocity based on the Bernoulli formula, equal to 15 m/s. The velocity distribution in the z-direction (height of the duct) is found to be almost symmetric, with a maximum value close to 8 m/s that corresponds to a mean value of 5.5 m/s, if we suppose that the profile is nearly parabolic. This result is drastically different from $V_{\mathrm{ref}} = 15\,\mathrm{m/s}$, which confirms that the losses in the pipe should be taken into account in the experiments.

4.2. Calculation of the head losses in the nozzle

In the present section, a method applicable with the three gases (air, Neon, CO_2) is proposed to determine the correct mean velocity at the nozzle outlet. In fact, hot-wire measurements can only be used in the case of air injection, because facilities to calibrate the wires for other gases were not available in the laboratory. So, air injection is considered here to validate the method.

The total pressure P_1 in the upstream chamber can be expressed as a function of the head losses ξ in the pipe and the total pressure P_2 at the nozzle outlet:

$$P_1 = P_2 + \xi, \tag{7}$$

where $P_2 = \frac{1}{2}\rho V_{\mathrm{ref}}^2$ with V_{ref} the mean velocity at the pipe outlet.

According to dimensional analysis rules, head losses ξ in a circular duct of diameter D and length L can be expressed in the following form:

$$\begin{aligned}\xi &= \frac{1}{2}\rho V_{\mathrm{ref}}^2 \Phi\left(\frac{L}{D}, \frac{UD}{v}\right)\\ &= \frac{1}{2}\rho V_{\mathrm{ref}}^2 \frac{L}{D}\Psi(\mathrm{Re}) = \frac{1}{2}\rho V_{\mathrm{ref}}^2 \frac{L}{D}\lambda,\end{aligned} \tag{8}$$

where $\lambda = \psi(\mathrm{Re})$ denotes the head losses coefficient classically evaluated in the case of a laminar flow by $\lambda = 64/\mathrm{Re}$. In the present configuration, the pipe is characterized by a rectangular cross-section instead of a circular one. Thus ξ must be scaled by a coefficient K that depends on the shape factor h/b of the pipe. Here $h/b = 0.6/20 = 0.03 \ll 1$, so K equals 1.5 (Idel'cik, 1986), and λ can be expressed as $\lambda = 96v/(DV_{\mathrm{ref}})$.

Therefore, ξ becomes

$$\xi = \frac{1}{2}\rho V_{\mathrm{ref}}^2 \frac{L}{D}\lambda = \frac{1}{2}\rho V_{\mathrm{ref}}^2 \frac{96vL}{D^2 V_{\mathrm{ref}}} \tag{9}$$

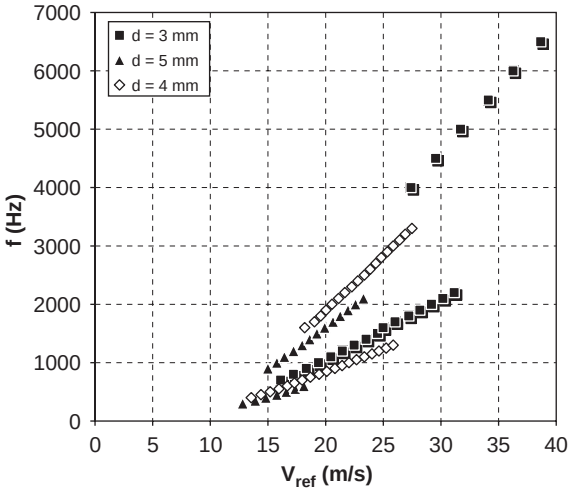

Fig. 5. Edge-tone frequencies versus mean velocity for three stand-off distances of the edge ($L = 50$ mm, head losses in the pipe are not considered).

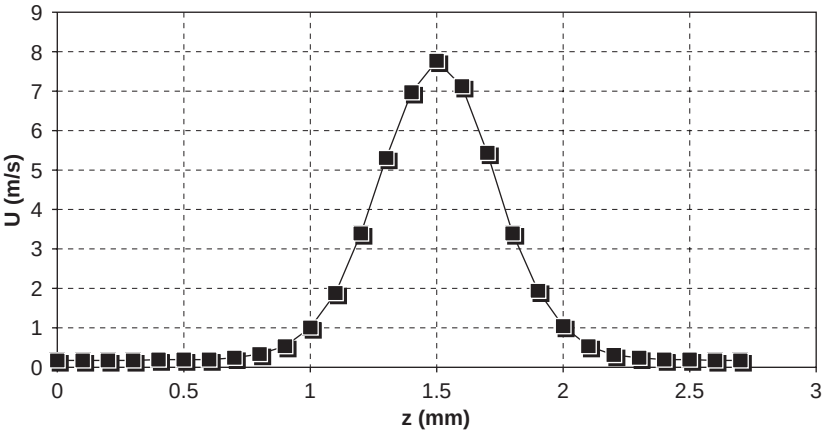

Fig. 6. Hot-wire transverse velocity profile at the flue outlet (no wedge, $L = 50$ mm, $V_{\mathrm{ref}} = 15$ m/s without considering head losses).

which gives the following relation for V_{ref}, using Eq. (7):

$$V_{\mathrm{ref}} = \frac{\xi D^2}{48\rho L v} = \frac{(P_1 - \frac{1}{2}\rho V_{\mathrm{ref}}^2)D^2}{48\rho L v}. \tag{10}$$

The resolution of Eq. (10) gives the value of the mean velocity V_{ref} in the duct for a fixed upstream pressure P_1. The values obtained are plotted in Fig. 7 as a function of P_1 and compared to: (i) the hot-wire measurements; (ii) the value derived from the total pressure measurement in the jet with the Pitot probe (see Section 2). The short pipe length ($L = 20$ mm) is used here, and it is checked with hot-wire acquisitions that the velocity profile at the duct outlet is parabolic.

A reliable agreement is obtained between the three results, with a maximum relative error of 5%. Although empirical coefficients in the literature have been applied without being strictly adapted to the present geometry, the proposed method can thus be used to calculate V_{ref}. It remains valid for injection of other gases, since it requires the measurement of the total pressure P_1 in the upstream chamber only, for given values of both the dynamic viscosity μ and density ρ. As a consequence, the method is applied to obtain all results presented in the following sections.

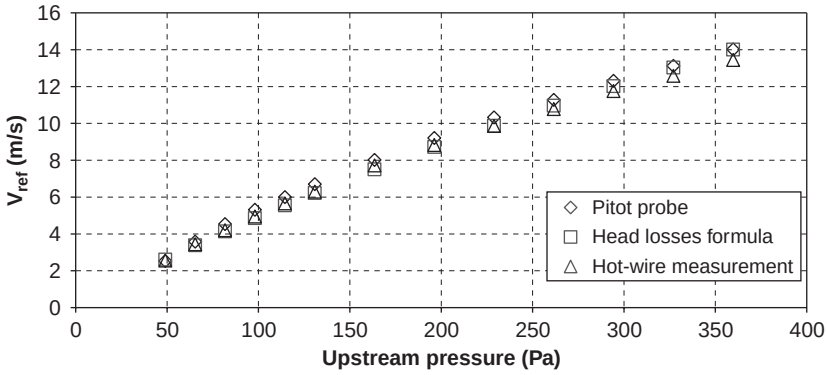

Fig. 7. Velocities obtained by the three methods for various chamber pressures (air injection).

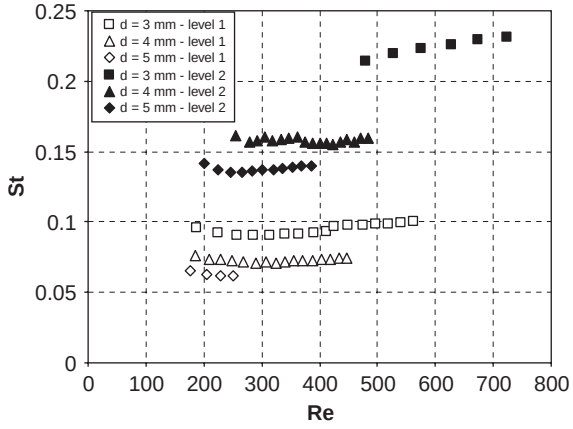

Fig. 8. Evolution of the Strouhal number for three stand-off distances d (frequency levels 1 and 2).

4.3. Validation of the measurements in air

The Strouhal numbers are plotted in Fig. 8 as a function of the Reynolds number in the case of air injection. The three values of the stand-off distance d are still considered (3, 4, and 5 mm), and the results obtained at frequency levels 1 and 2 are both reported. Nearly constant Strouhal numbers are systematically obtained for a given distance d. This result is consistent with the previous work of Holger et al. (1977), Crighton (1992), and Howe (1998).

In Fig. 9, The Strouhal numbers are plotted according to the ratio d/h. The present measurements are compared to the experimental data obtained previously in similar flow configurations by Brown (1935), Nyborg (1954), Brackenridge (1960), McCartney and Greber (1973), and reported by Holger et al. (1977). The theoretical law proposed by Holger, i.e. Eq. (1) with $C = 0.92(l + 0.4)$, is also drawn in Fig. 9 for levels $l = 1$ and 2. The empirical law proposed recently by Bamberger et al. (2001), i.e. Eq. (1) with $n = 1$ and $C = 0.495$, is also reported for level 1, since it is based on experiments performed in flow conditions very close to the present ones. The current results are in fair agreement with the other experimental data and also with the law derived by Bamberger et al. The discrepancies observed for both levels with the theoretical law proposed by Holger were already reported by Howe (1998). As a matter of fact, this law is much closer to the experimental measurements when the ratio d/h is increased.

4.4. Influence of the injection nozzle length and gas density

Experiments were performed with the three types of injected gas and two nozzle lengths in a range of reference velocity corresponding to the two first frequency levels ($3\,\mathrm{m/s} < V_{\mathrm{ref}} < 15\,\mathrm{m/s}$). In Fig. 10, the Strouhal numbers are

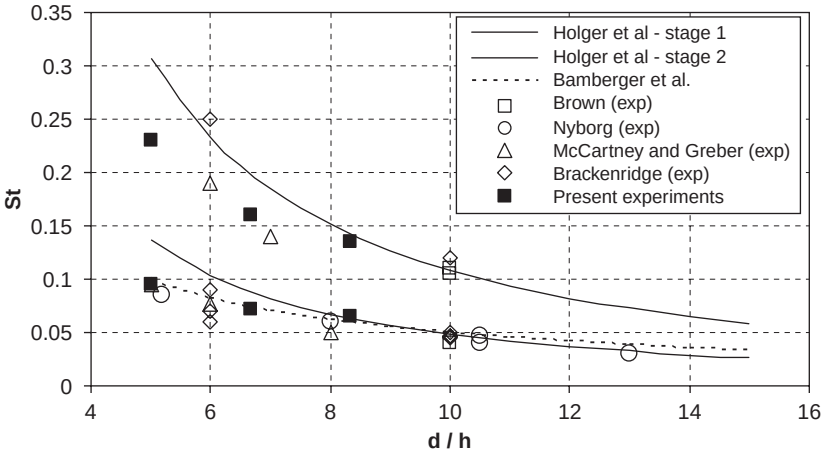

Fig. 9. Comparison of the Strouhal numbers with experimental and theoretical results of the literature (frequency stages 1 and 2).

plotted as a function of the Reynolds number. For each type of injection (Neon, air, CO_2), the data are drawn for both nozzle lengths and both frequency levels. It can be observed that the length of the injection duct has no significant influence on the Strouhal number values. This result contradicts the conclusions drawn by Ségoufin et al. (2004) from the use of different injection ducts. These authors found nonconstant Strouhal numbers depending much on the length of the injection duct. However, they did not take into account the head losses in their different ducts, so it can be inferred that they obtained the wrong reference velocities, as reported presently in Section 4.1. If their velocities were correct, they would probably get constant Strouhal numbers, with no influence of the inlet duct length.

Conversely, it can be deduced from Fig. 10 that the density of the injected gas has a significant influence on the Strouhal numbers. At the first frequency level, $St \approx 0.6$ in the case of Neon injection, 0.67 for air injection, and 0.77 for CO_2 injection. The same effect is obtained at the second frequency level, with Strouhal numbers equal to 0.135 with Neon injection, 0.16 with air injection, and 0.17 with CO_2 injection. So, injecting into a gas another gas with different properties (density and viscosity) noticeably alter the edge-tone phenomenon. For a given Reynolds number, the Strouhal number is higher with CO_2 injection (more dense than air) and lower with Neon injection (less dense than air). These results are compared in the next section with the numerical simulations, in order to propose an explanation for this behaviour.

5. Comparisons with numerical simulations

The model presented in Section 3 was applied to the flow conditions of the experiments. The unstable behaviour observed in the experiments is systematically well predicted in the calculations. The arrangement of the vortices at the edge tip is presented in Fig. 11 for Neon and CO_2 injection, successively. The flow predicted by the calculations is compared to the experimental visualizations at velocity $V_{ref} = 5\,m/s$. A fair agreement is obtained concerning the position and the shape of the vortices on both sides of the wedge. The lateral expansion of the vortices, which strongly depends on the gas nature, is also correctly simulated by the model. It can be observed that the Neon injection leads to a larger expansion of the vortices than the CO_2 injection, and also to more diffusion: this may be due to the difference in dynamic viscosity, which is much higher for Neon than for CO_2 (31.1 Pa s instead of 14.2 Pa s).

The first level frequencies are obtained in the simulations by analysing the time evolution of the far-field pressure (for example at the location of the microphone in the experiments). Then the Strouhal numbers predicted by the simulations are plotted in Fig. 12 according to the Reynolds number, for each type of injected gas. A reliable agreement with the experimental data is found in the whole range of Reynolds numbers. A maximum discrepancy of 6% is obtained in the case of CO_2 injection, for the highest velocities. In all other cases, the discrepancy is lower than 5%.

When the velocity is increased, a supplementary frequency can be detected in the flow. Its intensity progressively grows, and it finally becomes the dominant characteristic frequency of the periodic vortex shedding. Its value is consistent with the one measured in the experiments after the first frequency jump. However, no such jump can be determined numerically: only criteria based on the respective intensity of the two frequencies could be proposed to

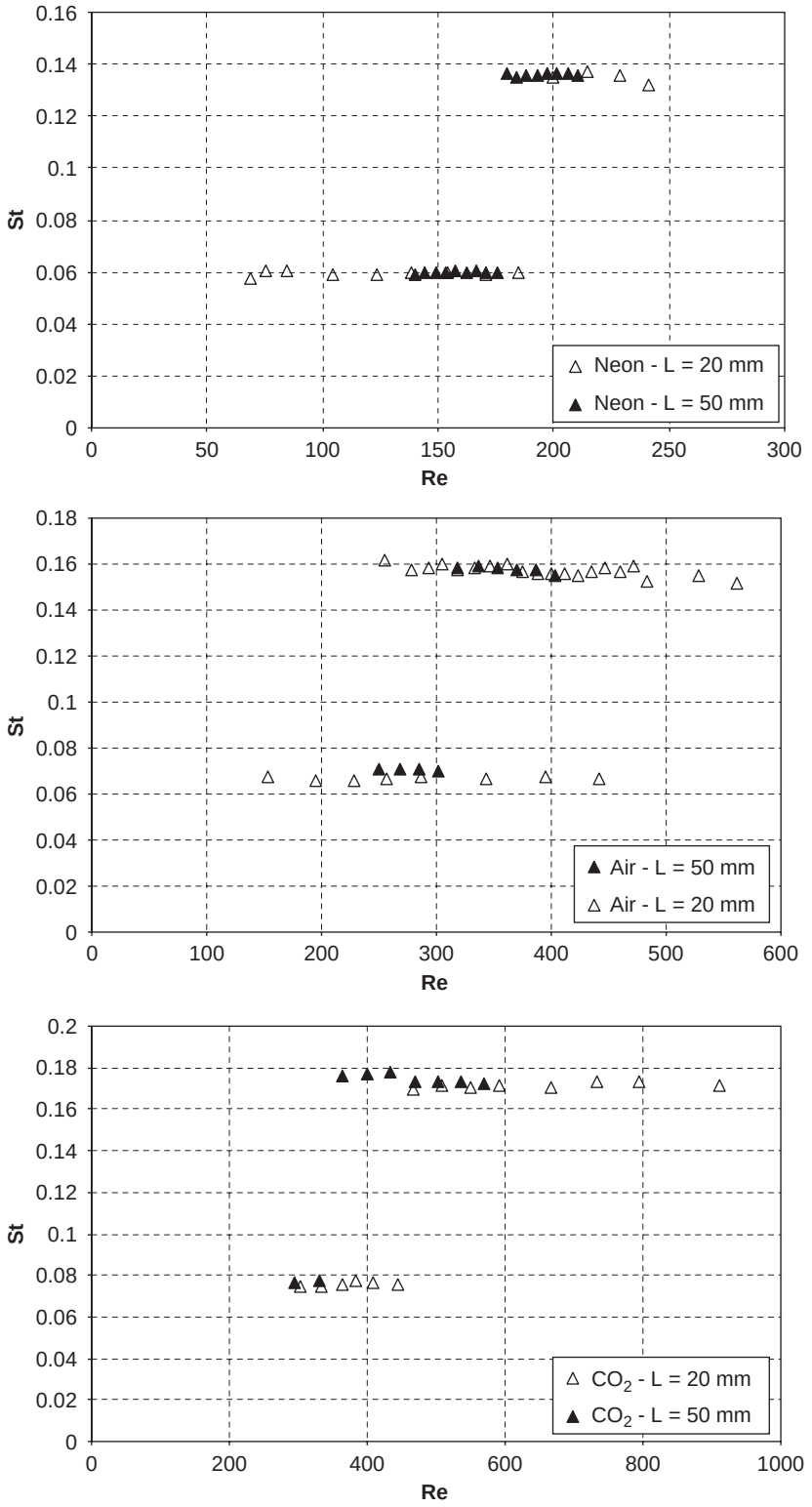

Fig. 10. Influence of the nozzle length and the density of the injected gas on the Strouhal number.

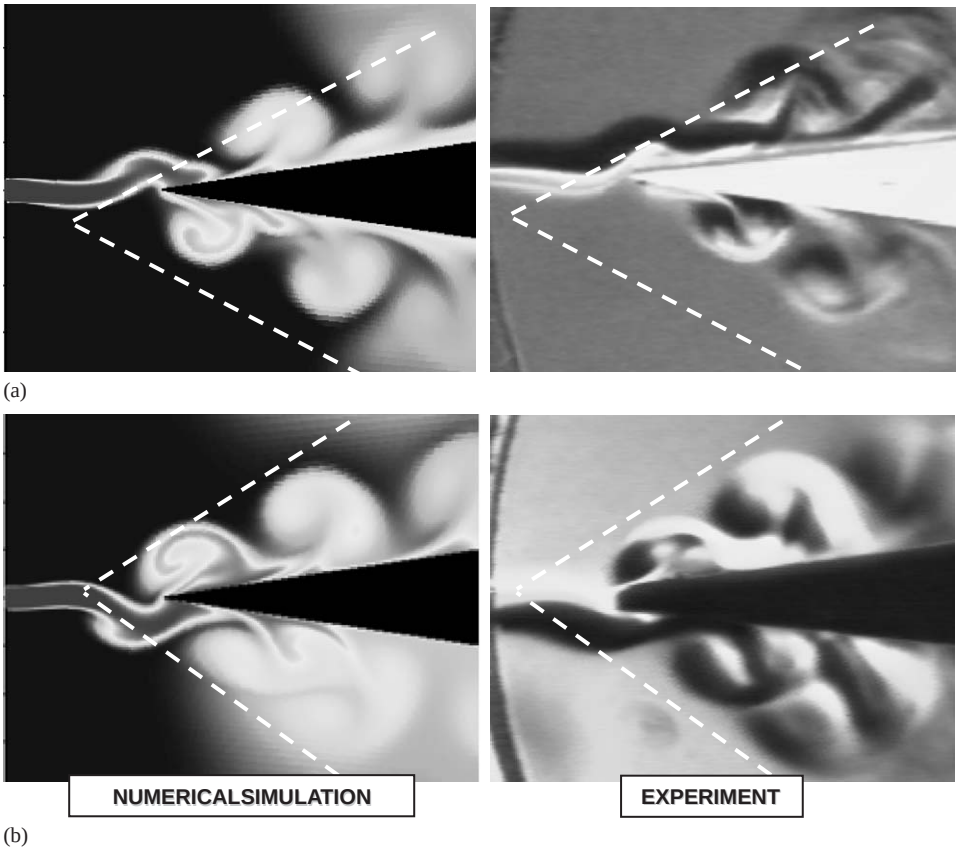

Fig. 11. Arrangement of the vortices for $V_{ref} = 5\,m/s$: (a) CO_2 and (b) Neon.

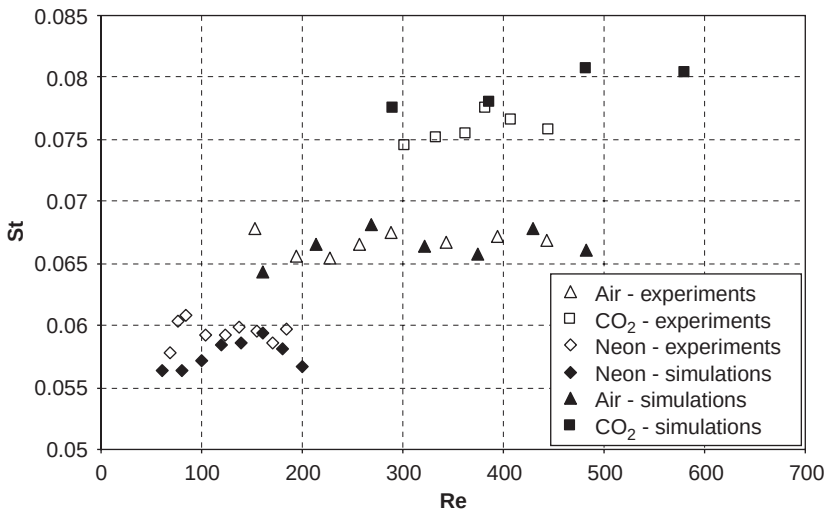

Fig. 12. Comparisons between experiments and calculation (frequency stage I).

predict the sound modification. Strouhal numbers based on this second category of frequencies are plotted in Fig. 13 and compared with the experimental data obtained at the second frequency level. A good agreement is obtained in the case of air injection, whereas significant discrepancies appear for Neon and CO_2. The difference reaches almost 7% in the case of Neon injection and 12% in the case of CO_2 injection.

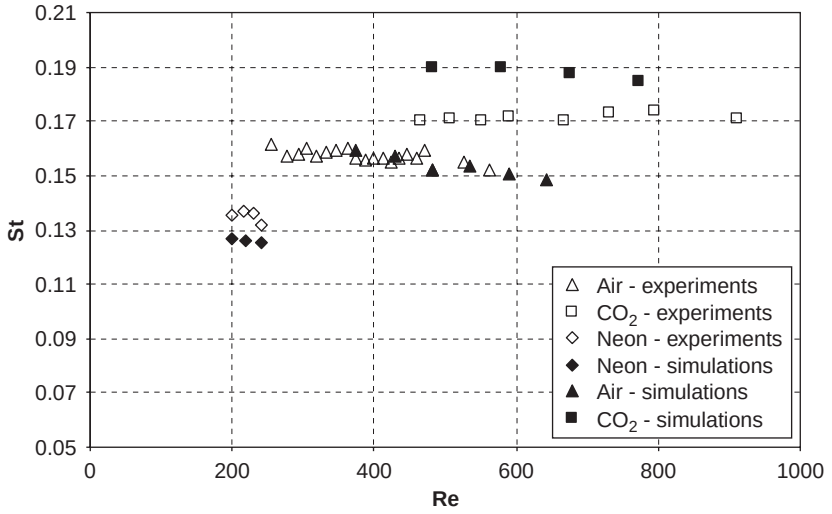

Fig. 13. Comparisons between experiments and calculation (frequency stage II).

The satisfactory agreement between the simulations and the experiments obtained for both frequency levels suggests that the density of the injected gas is a significant parameter of the edge-tone instability. However, the frequencies obtained in the different cases do not vary proportionally to the density of the jet. At a given Reynolds number, the Strouhal numbers obtained with the three different gases give the nearly constant ratios $St_{Neon}/St_{air} \approx 0.9$ and $St_{CO_2}/St_{air} \approx 1.1$, for both levels 1 and 2, while the density ratios are $\rho_{Neon}/\rho_{air} = 0.64$ and $\rho_{CO_2}/\rho_{air} = 1.52$. When Neon or CO_2 are injected, the generation of vortices at the tip of the wedge seems to become slightly different from simple air injection, and the Strouhal numbers do not anymore correspond to a Karman vortex street. The density discontinuity between the jet and the surrounding air suggests that the flow instability in the present case may be analogous to a Kelvin–Helmholtz instability. To investigate this point, a linear analysis of the flow instability is conducted in Section 6.

6. Linear analysis of the instability

In the present section it is assumed that the edge tone instability is similar to a Kelvin–Helmholtz instability, and we attempt to derive the frequency ratios from a linear stability analysis.

If a linear Kelvin–Helmholtz analysis is performed in the configuration of a flow discontinuity between two gases (velocity U_1 and density ρ_1, velocity U_2 and density ρ_2), the following standard dispersion relation is obtained between the instability frequency f and its wavelength Λ:

$$f\Lambda = \frac{\rho_1 U_1 + \rho_2 U_2}{(\rho_1 + \rho_2)}. \tag{11}$$

In the present case, U_1 is the mean jet velocity V_{ref}, $U_2 = 0$ is the velocity outside from the jet, ρ_1 is the density of the injected gas, and ρ_2 the one of the air. So, for the injection of air into air, Eq. (11) becomes simply:

$$f\Lambda = \frac{U}{2} = U_c, \tag{12}$$

where U_c denotes the convection velocity of the vortices, equal to half the reference velocity, according to the von Karman theory. In the case of CO_2 injection, for example, we obtain a slightly more complicated result:

$$f_{CO_2} = \frac{V_{ref}}{\Lambda} \frac{1}{1 + \rho_{air}/\rho_{CO_2}} \tag{13}$$

which gives finally the following ratio of frequencies between CO_2 injection and air injection:

$$\frac{f_{CO_2}}{f_{air}} = \frac{1 + \rho_{air}/\rho_{air}}{1 + \rho_{air}/\rho_{CO_2}} = \frac{2}{1 + 1/1.52} = 1.21$$

and for Neon injection, we obtain $f_{Neon}/f_{air} = 0.8$.

These values are still notably different from those obtained experimentally and numerically. However, the present linear analysis is based on a sharp discontinuity between the jet and the outer flow, whereas the real velocity distribution is almost parabolic in the present case. So the discrepancy between the theoretical and the experimental results may be reduced if the correct shapes of both the velocity and density profiles in the jet are taken into account in the theoretical development.

Let us consider the profiles of the nondimensional velocity component $U_0(y/L_{\mathrm{ref}}) = u/V_{\mathrm{ref}}$ and the nondimensional density $\alpha_0(y/L_{\mathrm{ref}}) = \rho/\rho_{\mathrm{air}}$ at mid-distance between the nozzle outlet and the wedge, before the flow instability starts (see Fig. 14 in the case of CO_2 injection). The nondimensional coordinates x/L_{ref} and y/L_{ref} are denoted by x_0 and y_0 below, respectively.

A linear perturbation is applied to the profiles

$$u = U_0 + \tilde{u}, \quad v = V_0 + \tilde{v}, \quad p = P_0 + \tilde{p}, \quad \alpha = \alpha_0 + \tilde{\alpha}.$$

The Euler equations are then linearized and we finally obtain

$$\begin{aligned}
&\frac{\partial \tilde{u}}{\partial x_0} + \frac{\partial \tilde{v}}{\partial y_0} = 0,\\
&\alpha_0 \frac{\partial \tilde{u}}{\partial t} + U_0 \frac{\partial \tilde{\alpha}}{\partial t} + U_0 \alpha_0 \frac{\partial \tilde{u}}{\partial x_0} + U_0^2 \frac{\partial \tilde{\alpha}}{\partial x_0}\\
&\quad + \tilde{v} \frac{\partial}{\partial y_0}(\alpha_0 U_0) = -\frac{\partial \tilde{p}}{\partial x_0},\\
&\alpha_0 \frac{\partial \tilde{v}}{\partial t} + U_0 \alpha_0 \frac{\partial \tilde{v}}{\partial x_0} = -\frac{\partial \tilde{p}}{\partial y_0},\\
&\frac{\partial \tilde{\alpha}}{\partial t} + U_0 \frac{\partial \tilde{\alpha}}{\partial x_0} + \tilde{v} \frac{\partial \alpha_0}{\partial y_0} = 0.
\end{aligned} \tag{14}$$

The first equation is the continuity equation, the second and the third one are the momentum equations in directions x and y, and the last one is the transport equation for $\tilde{\alpha}$.

Since the flow is assumed to be incompressible, we use hereafter a function ψ defined by $u = \partial\psi/\partial y_0$ and $v = -\partial\psi/\partial x_0$. As a first approximation, we neglect the variations of $\tilde{\alpha}$ in the momentum equations and thus, by eliminating the pressure in the second and the third equations of the previous system, we obtain

$$\begin{aligned}
&\left(\frac{\partial}{\partial t} + U_0 \alpha_0 \frac{\partial}{\partial x_0}\right)\left(\frac{\partial^2 \tilde{\psi}}{\partial x_0^2} + \frac{\partial^2 \tilde{\psi}}{\partial y_0^2}\right) - \frac{\partial}{\partial y_0^2}(\alpha_0 U_0)\frac{\partial \tilde{\psi}}{\partial x_0} = 0,\\
&\frac{\partial \tilde{\alpha}}{\partial t} + U_0 \frac{\partial \tilde{\alpha}}{\partial x_0} - \left(\frac{\partial \alpha_0}{\partial y_0}\right)\frac{\partial \tilde{\psi}}{\partial x_0} = 0.
\end{aligned} \tag{15}$$

We are looking hereafter for normal modes of the form

$$\tilde{\psi} = \theta_1(y_0)\mathrm{e}^{\mathrm{i}(kx_0 - \omega t)}, \quad \tilde{\alpha} = \theta_2(y_0)\mathrm{e}^{\mathrm{i}(kx_0 - \omega t)}$$

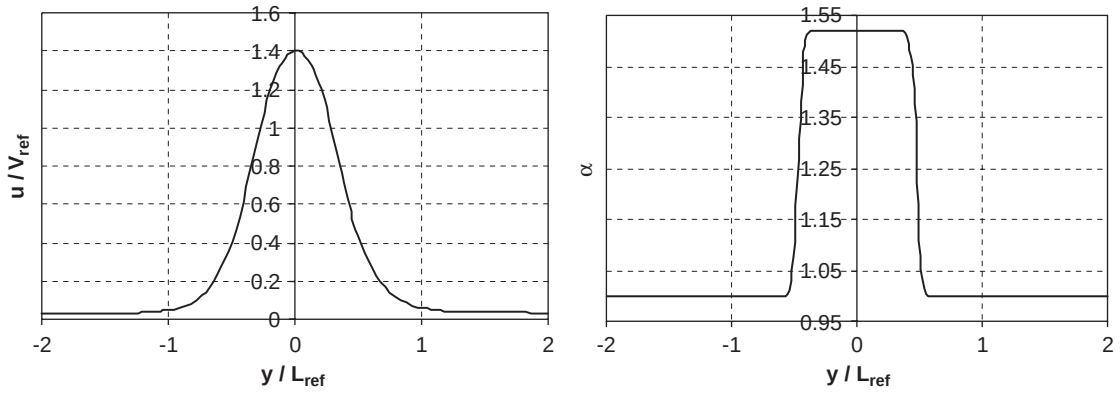

Fig. 14. Profiles of velocity and density in the jet at $x/L_{\mathrm{ref}} \approx 3$ (CO_2 injection).

with k the nondimensional real wavenumber and ω the complex temporal frequency. This gives the following system of two equations to be solved:

$$\begin{aligned}(U_0\alpha_0 - c)\left(\frac{\partial^2\theta_1}{\partial y_0^2} - k^2\theta_1\right) - \frac{d^2(U_0\alpha_0)}{dy_0^2}\,\theta_1 = 0,\\ (U_0 - c)\theta_2 - \frac{d\alpha_0}{dy_0}\,\theta_1 = 0,\end{aligned} \tag{16}$$

where c is the wave propagation speed $c = \omega/k$.

Since the density fluctuations in the momentum equation have been neglected, the first equation is uncoupled from the second one and it can be solved independently, so long as the functions $U_0\alpha_0(y_0)$ and its second derivative are available. The profile $U_0\alpha_0$ (y_0) obtained numerically (see Fig. 14) is presently approximated by a function F of the form: $F(y_0) = A\ \tan h(By_0^2) + C$, where A, B, C are three constants that depend on the injected gas. Fig. 15 shows in the case of a CO_2 jet that the approximation of $U_0\alpha_0$ (y_0) by the function F is satisfactory.

Outside from the jet, $F''(y_0)$ rapidly decreases close to zero, and the first equation of the system (16) can be expressed in the form

$$\left(\frac{\partial^2\theta_1}{\partial y_0^2} - k^2\theta_1\right) = 0, \tag{17}$$

of which solution is $C_1e^{ky_0}$ if $y_0 \leqslant 0$ and $C_2e^{-ky_0}$ if $y_0 \geqslant 0$, with C_1 and C_2 constants. So, the boundary condition for θ_1'/θ_1 far from the jet is $+k$ for $y_0 \leqslant 0$ and $-k$ for $y_0 \geqslant 0$.

Eq. (1) of system (16) is integrated numerically with a Runge–Kutta scheme of fourth-order, between $y_{0\min}$ and $y_{0\max}$. The integration starts in $y_{0\min}$ by imposing the boundary conditions $\theta_1 = 10^{-4}$ and $\theta_1'/\theta_1 = k$. Only the value of wavenumber k corresponding to the wavelength derived from the standoff distance d between the nozzle and the edge is considered, and the value of c is adjusted so that the boundary conditions for θ_1 and θ_1'/θ_1 in $y_{0\max}$ are satisfied. The real part of c gives the frequency of the instability. This process is repeated for the injection of the three gases. Several values of the integration limits $y_{0\min}$ and $y_{0\max}$, from ± 2 to ± 5 are also tested, since these parameters seem to significantly influence the frequency obtained. However, the ratios of the frequencies obtained in air, Neon and CO_2 remain almost constant, whatever the values of $y_{0\min}$ and $y_{0\max}$ (see Table 2):

$$f_{\text{Neon}}/f_{\text{air}} = 0.89 \text{ and } f_{CO_2}/f_{\text{air}} = 1.09.$$

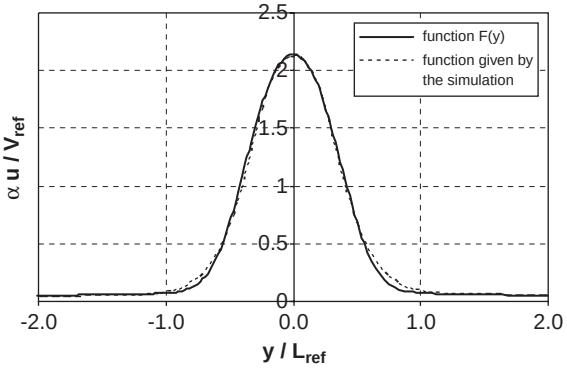

Fig. 15. Approximation of $\alpha u/V_{\text{ref}}$ (case of CO_2 injection).

Table 2
Ratios of the frequencies for different values of $y_{0\min}$, $y_{0\max}$

$y_{0\min}/y_{0\max}$	$f_{\text{Neon}}/f_{\text{air}}$	f_{CO_2}/f_{air}
−2/2	0.87	1.13
−3/3	0.91	1.09
−4/4	0.90	1.09
−5/5	0.89	1.10

These values are very close to those measured experimentally, which confirms that the shape of the velocity and density profiles inside the jet is of prime importance in the linear stability analysis. With a sharp discontinuity of velocities at the nozzle outlet, the basic effect of the density of the injected gas (higher frequency for a denser gas, lower density for a less dense gas) is overestimated. In reality, the parabolic velocity profile increases the mixing of the two gases between the duct outlet and the wedge, and thus somehow counterbalances the previous basic effect. Indeed, the local density gradients when the flow reaches the wedge tip have significantly decreased, compared with the initial sharp density discontinuity. Taking into account some realistic velocity and density profiles in the Kelvin–Helmholtz linear analysis enables one to obtain better velocity and density gradients at the limit of the jet, and thus more realistic momentum flow rates.

The reliable agreement which is finally found between experimental, numerical, and theoretical results concerning the frequency ratios suggests that the edge-tone phenomenon can be interpreted as a Kelvin–Helmholtz instability developing in the jet mixing layers.

7. Conclusions

The edge-tone phenomenon has been investigated with injections of different gases into the air, in order to determine the influence of the gas density on both the flow arrangement and the vortex shedding frequency. Special attention has been paid to the determination of the mean velocity at the nozzle outlet. It has been shown that if the head losses in the nozzle are correctly taken into account, the length of the nozzle has nearly no influence on the results. Conversely, a significant effect of the density of the injected gas has been pointed out concerning the growth of the vortices on both sides of the edge. Moreover, the Strouhal numbers derived from the frequencies of vortex shedding have been found higher in CO_2 than in air (ratio 1.1) and lower in Neon (ratio 0.9), for both levels 1 and 2. A two-dimensional numerical model has also been applied to the simulation of the edge-tone. A reliable agreement between the experiments and the calculations has been obtained for level 1. Frequencies of level 2 have also been detected in the numerical simulations, with a reliable accuracy in the case of air injection, about 7% of error for Neon injection, and 12% for CO_2 injection.

This modification of the Strouhal numbers shows that the edge-tone instability, when it is based on the injection of one gas into another, cannot be considered anymore as a Karman vortex street. To investigate this point, an analogy between the edge-tone instability and the Kelvin–Helmholtz instability has been proposed and discussed. If sharp discontinuities of both velocity and density across the jet are considered, this results in a classical dispersion relation, which does not correctly account for the evolution of the jet oscillation frequency with the nature of the injected gas. However, this relation does not take into account the significant mixing of the injected gas with the air between the nozzle outlet and the wedge tip, which can be clearly observed in the results of the numerical simulations. An attempt to include this mixing was performed by considering more realistic velocity and density profiles, based on the numerical simulations, in the linear analysis. Then, the results are notably improved: at a given reference velocity, the ratios $f_{\mathrm{Neon}}/f_{\mathrm{air}}$ and $f_{\mathrm{CO_2}}/f_{\mathrm{air}}$ become in close agreement with the experimental and numerical data. It can thus be inferred that the mixing of the gases is as important as the initial density ratio in the modification of the vortex frequencies. If this mixing is included in the linear analysis by using velocity and density profiles close to the real ones, the frequencies resulting from the edge-tone instability can be derived from a Kelvin–Helmholtz linear analysis.

Acknowledgements

The numerical model was initially developed in the LEGI laboratory (Laboratoire des Ecoulements Géophysiques et Industriels, Grenoble, France) for 20 years with successive work by Y. Delannoy (currently assistant professor at the Institut National Polytechnique, Grenoble) and J.-L. Reboud (currently professor at Joseph Fourier University, Grenoble). This research was performed in the framework of collaboration between the LEGI and the CNES (Centre National d'Etudes Spatiales) for cavitating flow applications.

References

Bamberger, A., Bänsch, E., Siebert, K.G., 2001. Experimental and numerical investigation of edge tones. Technical Report Preprint no. 681, Weierstrass Institut fur Angewandte Analysis und Stochastik, Berlin.

Benton, W.E., 1925. On edge-tones. Proceedings of the Physical Society of London 38, 109–126.

Brackenridge, J.B., 1960. Transverse oscillations of a liquid jet. Journal of the Acoustical Society of America 32, 1237.
Brown, G.B., 1935. On vortex motion in gaseous jets and the origin of their sensitivity to sound. Proceedings of the Physical Society of London 47, 703.
Brown, G.B., 1937. The vortex motion causing edge tones. Proceedings of the Physical Society of London 49, 493–507.
Coutier-Delgosha, O., Devillers, J.-F., Chaigne, A., 2005. A joint experimental and numerical study of the edgetone phenomenon. Acta Acustica, submitted for publication.
Crighton, D.G., 1992. The edge tone feedback cycle; linear theory for the operating stages. Journal of Fluid Mechanics 234, 361–391.
Holger, D.K., Wilson, T.A., Beavers, G.S., 1977. Fluid Mechanics of the edgetone. Journal of the Acoustical Society of America 62, 1116–1128.
Howe, M.S., 1998. Acoustics of Fluid Structure Interactions. Cambridge University Press, Cambridge.
Idel'cik, I.E., 1986. Memento des Pertes de Charge. Editions Eyrolles, Paris.
Maurel, A., Ern, P., Zielinska, B.J.A., Wesfreid, J.E., 1996. Experimental study of self-sustained oscillations in a confined jet. Physical Review E 54, 3643–3651.
McCartney, M.S., Greber, I., 1973. An experimental and theoretical investigation of the edgetone phenomenon, FTAS TR-73-87, Case Western Reserve University.
Merzkirch, W., 1987. Flow Visualization, Second ed. Academic Press, London.
Nyborg, W., 1954. Self-maintained oscillations in a jet edge system. Journal of the Acoustical Society of America 26, 174.
Patankar, S.V., 1981. Numerical Heat Transfer and Fluid Flow. Hemisphere Publishing Corporation, Washington.
Pope, S.B., 1978. The calculation of turbulent recirculating flow in general orthogonal coordinates. Journal of Computational Physics 26, 197.
Powell, A., 1953. On edgetones and associated phenomena. Acustica 3, 233–244.
Schlichting, H., 1979. Boundary Layer Theory, Seventh ed. McGraw-Hill, New York.
Ségoufin, C., Fabre, B., Verge, M-P., Hirschberg, A., Wijnands, A.P.J., 2000. Experimental study of the mouth geometry on sound production in a recorder-like instrument: windway length and chamfers. Acta Acustica 86, 649–661.
Ségoufin, C., Fabre, B., de Lacombe, L., 2004. Experimental investigation of the flue channel geometry influence on edge-tone oscillations. Acta Acustica 90, 966–975.
Yoshikawa, S., 2000. A pictorial analysis of jet and vortex behaviours during attack transients in organ pipe models. Acustica 86, 623–633.
Zhu, J., 1991. A low diffusive and oscillation-free convection scheme. Communications in Applied Numerical Methods 7, 225–232.